Open access • Journal Article • DOI:10.1088/0953-4075/48/21/214001

Probing Wavepacket Dynamics using Ultrafast X-ray Spectroscopy

Gloria Capano, Christopher J. Milne, Majed Chergui, Ursula Rothlisberger ...+2 more authors

Institutions: École Polytechnique Fédérale de Lausanne, Paul Scherrer Institute, IBM

Published on: 23 Sep 2015 - Journal of Physics B (IOP Publishing)

Topics: Excited state

Capano G, Milne CJ, Chergui M, Rothlisberger U, Tavernelli I, Penfold TJ. **Probing Wavepacket Dynamics using Ultrafast X-ray Spectroscopy**. ***Journal of Physics B*** **2015, 48(21), 1-11.**

Probing Wavepacket Dynamics using Ultrafast X-ray Spectroscopy

G. Capano[1], C.J. Milne[2] M. Chergui[1], U. Rothlisberger[3], I. Tavernelli[4] and T.J. Penfold[2]

1 Ecole polytechnique Fédérale de Lausanne, Laboratoire de spectroscopie ultrarapide, ISIC, FSB, CH-1015 Lausanne, Switzerland
2 SwissFEL, Paul Scherrer Inst, CH-5232 Villigen, Switzerland.
3 Ecole polytechnique Fédérale de Lausanne, Laboratoire de chimie et biochimie computationnelles, ISIC, FSB-BSP, CH-1015 Lausanne, Switzerland
4 IBM Research GmbH, Zurich Research Laboratory 8803 Rueschlikon Switzerland.

E-mail: `tom.penfold@ncl.ac.uk`

Submitted to: *J. Phys. B: At. Mol. Phys.*

Abstract. The advent of X-ray Free Electron Lasers (X-FELs) is providing new opportunities for probing the ultrafast excited state dynamics using structurally sensitive techniques. Herein we use excited state wavepacket dynamics of a prototypical Cu(I)-phenanthroline complex, $[Cu(dmp)_2]^+$ (dmp = 2,9-dimethyl-1,10-phenanthroline) to investigate how femtosecond vibrational and electronic relaxation is translated into transient X-ray absorption (XAS) and emission (XES). Using realistic experimental parameters we also derive the anticipated signal strengths for these transient features. This indicates that although recording a signal capturing the strongest transient (i.e. excited state - ground state) changes will be possible for all cases, only with X-ray Absorption Near-Edge Structure (XANES) and Extended X-ray Absorption Fine Structure (EXAFS) will it be possible to resolve the fine details associated with the wavepacket dynamics within realistic experimental acquisition times.

1. Introduction

Probing ultrafast non-equilibrium dynamics became possible with the advent of ultrafast time-resolved linear and non-linear optical spectroscopies [1, 2]. However, because optical spectroscopy consists of transitions between delocalised valence states, the link between the spectroscopic observable and structure is ambiguous for systems of more than one nuclear degree of freedom, i.e. >2 atoms. To overcome this, the last decades have witnessed a significant research effort aimed at exploiting short wavelength probe pulses to achieve direct structural sensitivity in time-resolved pump-probe experiments. This has led to the development of time-resolved diffraction methods using X-rays [3, 4, 5] or electrons [6, 7] and core level spectroscopies using either X-rays [8, 9, 10, 11] or electrons [12, 13]

For the implementation of time-resolved X-ray spectroscopy, the focus of this present work, third generation light sources are most suited because of their wide tuneability, stability and high photon flux. However, for normal operational modes, the X-ray pulses from these light sources have a temporal width of 50-100 ps. They are therefore unable to probe the initial ultrafast dynamics that can often be critical in determining the outcome of non-equilibrium dynamics. While this can, to a certain extent, be overcome using the laser-slicing scheme [14] which has been used to demonstrate femtosecond X-ray spectroscopy [15, 16, 17, 18], these experiments are extremely challenging due to low photon counts. With an X-ray flux per pulse that is typically 10-11 orders of magnitude higher than the laser-slicing scheme, X-ray Free electron lasers (X-FELs) [19] offer new perspectives for performing ultrafast X-ray experiments. Indeed, femtosecond X-ray spectroscopy at X-FELs has been demonstrated for photoexcited $[Fe(bpy)_3]^{2+}$ [20, 21], $[Fe(phen)_2(NCS)_2]$[22] $[Fe(C_2O_4)_3]^{3-}$ [23] and $Fe(CO)_5$ [24].

These studies have been used to shed light into the evolving electronic structure, changing spin states and overall structural changes occurring after photoexcitation. However, none of these studies have probed the nuclear wavepacket dynamics, which

is commonly elucidated from femtosecond optical spectroscopy [25, 26]. Indeed directly observing signatures of (coherent) vibrational dynamics, electronic relaxation, intramolecular energy redistribution and vibrational cooling can shed important insight into how a particular system dissipates the energy after photoexcitation. Consequently, the absence of these dynamics in any time-resolved X-ray spectroscopic experiment reported to date poses a number of questions: i) What is the sensitivity of X-ray spectroscopic techniques to wavepacket dynamics? ii) What is the measurement sensitivity and therefore number of photons required to successfully observe these dynamics? iii) What is the best X-ray spectroscopic technique to observe these dynamics?

To address these questions, in this paper we use first principles quantum dynamics simulations [27, 28] of a prototypical Cu(I)-phenanthroline complex, $[Cu(dmp)_2]^+$ (dmp = 2,9-dimethyl-1,10-phenanthroline), initiated after photoexcitation into the optically bright metal-to-ligand charge-transfer (MLCT) state to investigate how femtosecond nuclear wavepacket dynamics are reflected in X-ray spectroscopic signals. This is achieved by studying the Extended X-ray Absorption Fine Structure (EXAFS), pre-edge X-ray Absorption Near-Edge Structure (XANES), K$\alpha_{1,2}$, K$\beta_{1,3}$ and K$_{\beta_{2,5}}$ (sometimes referred to as valence-to-core) X-ray emission (XES) spectra. Subsequently, using realistic experimental parameters we derive the anticipated signal strengths for these transient (i.e. excited state - ground state) features. For the present complex, these simulations show that while recording a signal capturing the strongest transient changes is possible for each spectroscopic method, only for XANES and EXAFS will it be possible to resolve the fine details associated with wavepacket dynamics within realistic experimental acquisition times.

2. Theory and computational details

2.1. Quantum Dynamics of $[Cu(dmp)_2]^+$

In this work we derive ultrafast X-ray spectroscopic signals from our recent quantum dynamics of a prototypical Cu(I)-phenanthroline complex, $[Cu(dmp)_2]^+$ [27, 28]. The ultrafast dynamics of $[Cu(dmp)_2]^+$ have previously been well characterised using optical absorption and emission spectroscopies [29, 30, 31, 32, 33, 34]. The general picture that emerges from these studies indicates that following photoexcitation, the complex relaxes into the lowest singlet excited state in ∼100 fs. This is followed by a structural distortion (flattening of the dihedral angle between the ligands, see Figure 1a), and intersystem crossing (ISC) to the lowest triplet state T_1 [34]. Of particular relevance to the present work, Tahara and co-workers [32, 33, 34] have demonstrated the presence of distinct wavepacket dynamics occurring in the excited state. These coherent vibrational dynamics are dominated by a vibrational mode with frequency 125 cm^{-1} (period of ∼300 fs), which was assigned to a breathing mode of the complex that causes a symmetric stretching of the four Cu-N bonds [33].

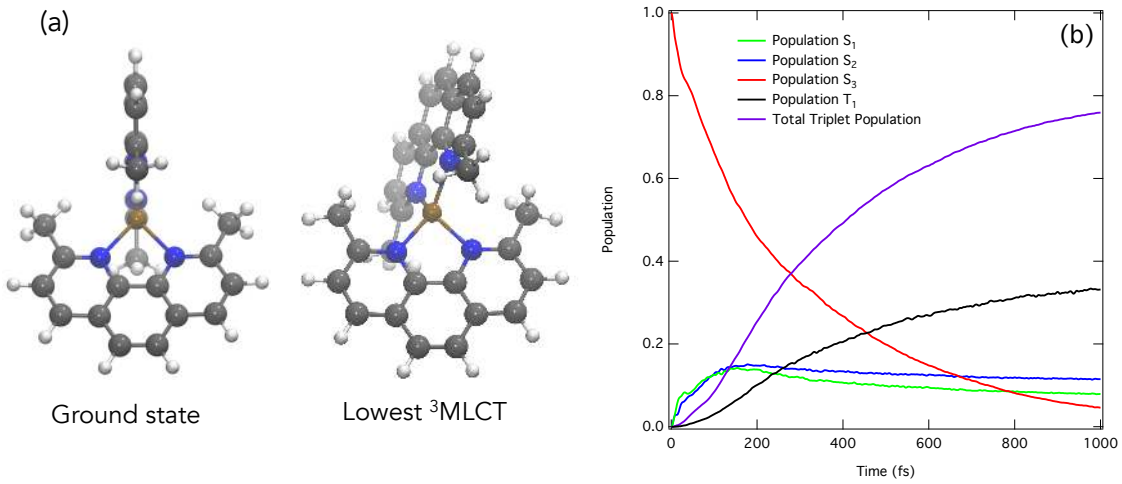

Figure 1. (a) DFT (B3LYP)-optimized geometry of the ground state (left) and lowest triplet state (right) of $[Cu(dmp)_2]^+$. (b) Relative diabatic state populations of S_1 (blue), S_2 (green), S_3 (red), T_1 (black) and all the triplet (T1-T4) states (purple), for 1 ps following photoexcitation. Figure replotted from ref. [28]

The quantum dynamics used herein are presented in detail in refs [27, 28] and were performed using the Heidelberg Multi Configuration Time Dependent Hartree (MCTDH) package [35, 36]. The Hamiltonian was described using the vibronic coupling model [37]. It included 8 nuclear degrees of freedom, the three lowest singlet states and the four lowest triplet states [27]. The population kinetics during the first picosecond after photoexcitation are shown in Figure 1b. After photoexcitation, which populates the S_3 state (red trace, Figure 1b), we observe rapid population decay into the S_2 and S_1 states. Due to a degeneracy of these states with the lowest lying triplet states, there is rapid intersystem crossing into the triplet manifold (purple line) and after 1 ps ∼80% of the wavepacket is in the triplet states. Of this population, just under half is in the T_1 state. Further details of the quantum dynamics simulations used in this study can be found in refs [27, 28]

As discussed below, much of this study focuses upon the dynamics along modes ν_8 and ν_{21} in the T_1 state. ν_8 is the totally symmetric breathing mode responsible for the contraction of the Cu-N distance in the excited state and ν_{21}, is the mode associated with the pseudo Jahn-Teller (PJT) distortion. Figure 2 shows the position and width of the wavepacket in the T_1 state along these modes. The position of the wavepacket along ν_8 shows an oscillation with a period of ∼300 fs in good agreement with the wavepacket dynamics reported by Tahara *et al.* [55], The width only shows small oscillators, and remains roughly constant throughout the first picosecond. In contrast, ν_{21} exhibits no significant displacement from the Franck-Condon geometry. Instead, due to the vibrational hot system, in these states the dynamics are reflected in the width of the wavepacket, rather than position. Here, at early times we observe a large increase in the width of the wavepacket along ν_{21}. The gradual decrease in this width is highlighting

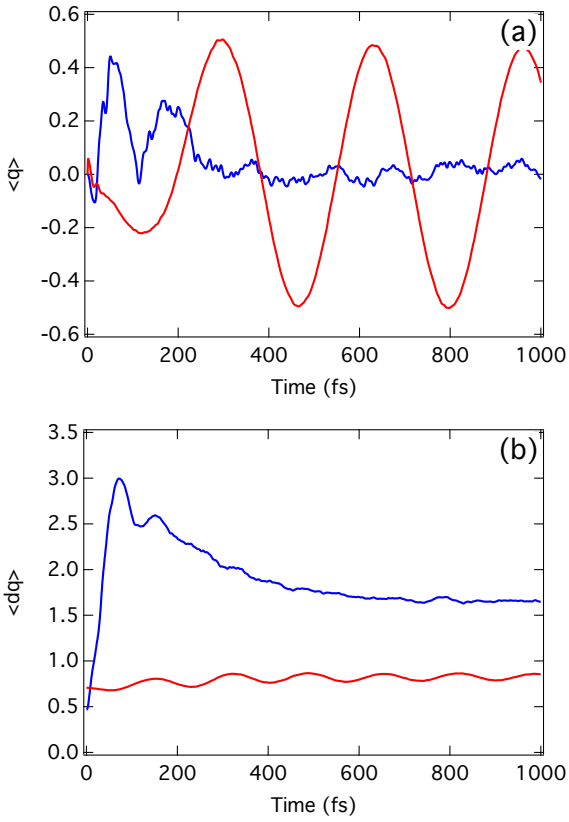

Figure 2. Expectation value of the position, $\langle q \rangle$ (a), and of the width, $\langle dq \rangle$ (b), of the wavepacket in the T_1 state. Colors: red, ν_8; blue, ν_{21}.

the beginning of vibrational relaxation.

2.2. Simulations of the time-resolved spectra

The X-ray spectrum of the non-stationary wavepacket is calculated as the weighted sum of the spectra calculated at each grid point used to describe the nuclear wavepacket. The weighting corresponds to the magnitude of the nuclear wavepacket at that grid point. For the EXAFS spectra, a sum over each electronic state was also performed, thus achieving a description of the full nuclear wavepacket. All of the other spectra (pre-edge XANES and XES) only considered the wavepacket, and thus the dynamics, on the T_1 state.

This is because, in contrast to EXAFS spectra, the valence electronic structure is expected to influence the spectrum, meaning that for the excited states (i.e. S_1, S_2, S_3 and T_2, T_3, T_4), one must simulate the core-level spectrum of each excited state. Due to the two excitation steps, the transition dipole matrix elements between the valence excited state and the final core-excited state cannot be computed within linear response theories, such as Linear response-time-dependent density functional theory (LR-TDDFT). However, since DFT is rigorously valid for the lowest state of a given

spin, we are able to simulate the T_1 state.

At present, the most rigorous approach of simulating the core-level spectra of electronically excited states is Restricted Active Space Self Consistent Field (RASSCF) method [38]. However, since these calculations are extremely computationally intensive they are unrealistic to describe the time-evolution of a nuclear wavepacket. Consequently, this approach is best applied to probe selected important points of the dynamics, as recently demonstrated in the study of photoexcited $Fe(CO)_5$ [24]. An alternative approximate way to address the excited state is using a ΔSCF approach, such as the maximum overlap method (MOM) [39, 40]. However, this requires that the excited state is well describe by a single electron excitation, such as a HOMO-LUMO transition. Unfortunately this is not the case for the present system. In addition, the character of the excited states changes along the main reaction path making it impossible to assign a single configuration to represent each of the excited states.

The EXAFS spectra at each grid point were calculated with the FEFF9 package [41] using the path expansion multiple scattering approach and a self-consistent field (SCF) potential. All scattering pathways shorter than 6 Å were included. The XAS and XES spectra were computed within the one-electron approach [42, 43] as implemented in the ORCA [44] quantum chemistry package. Computations used the BP86 functional [45, 46] and the def2-TZVP basis set [47, 48]. All of the calculations included spin orbit coupling (SOC), for which the SOC operator is approximated by the spin-orbit mean field method (SOMF) [49]. A Lorentzian lifetime broadening with full-width half maximum (FWHM) of 1.89 eV was applied to the pre-edge XANES, while a Lorentzian broadening with FWHM of 2.5 eV was used for the XES spectra.

Finally, for both the XAS and XES spectra, the relative energies of the calculated transition are generally well reproduced compared to experiment. However, it is well documented that the absolute transition energies are usually in poor agreement [50]. This failure stems from the approximate exchange description within the exchange-correlation functionals and is associated with the self interaction error (SIE) [51]. This is usually corrected by applying a constant shift to the spectrum *a posteriori* [52, 53]. In this case, as the spectra presented herein are not directly compared to experimental data, these shifts have not been included.

3. Results

In the following sections, we present the simulations of the EXAFS, pre-edge XANES and XES spectra. Then, using the calculated signal magnitudes, we derive the anticipated feasibility of these techniques to probe the wavepacket dynamics.

3.1. EXAFS

The ground state EXAFS spectrum of $[Cu(dmp)_2]^+$ [54] compared to the spectrum simulated using the ground state wavepacket is shown in Figure S1. Although the

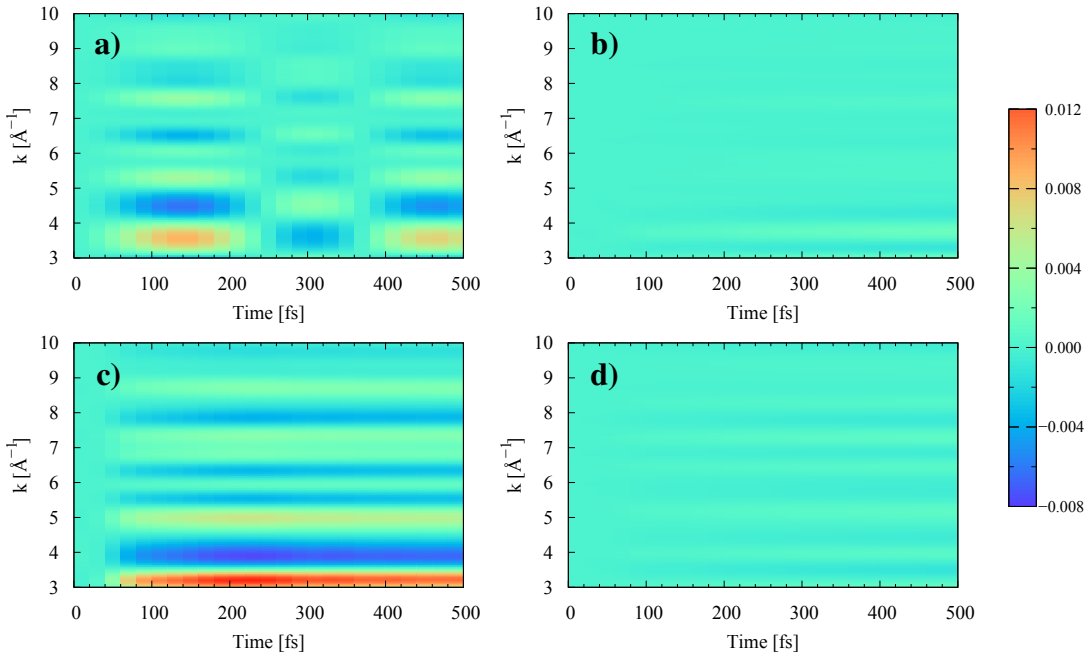

Figure 3. The simulated transient Cu K-edge EXAFS spectrum, $\Delta\chi$, of $[Cu(dmp)_2]^+$ for the first 500 fs after photoexcitation. In each case the spectra are calculated using the nuclear wavepacket dynamics along one degree of freedom; ν_8 (a), ν_{19} (b), ν_{21} (c), ν_{25} (d).

simulated spectrum is slightly more structured than the experimental spectrum, fairly good agreement between the two is observed with the main features, especially those at low k, well captured. As previously reported [54], this EXAFS spectrum is largely dependent on the Cu-N distance, which is 2.09 Å in the ground state.

Figure 3 shows the transient EXAFS spectrum for the first 500 fs of the photoexcited dynamics projected along 4 (ν_8, ν_{19}, ν_{21}, ν_{25}) of the 8 nuclear degrees of freedom included in the model Hamiltonian. This shows that two modes, ν_8 and ν_{21}, would be expected to dominate the transient features. The other two modes, ν_{19}, ν_{25} have a weak signal as they are not strongly displaced from their ground state configuration during the dynamics [28]. Of the two active modes, ν_8 is the totally symmetric breathing mode responsible for the contraction of the Cu-N distance in the excited state. This shows an oscillation, caused by a phase shift in the transient EXAFS spectrum, with a period of ∼300 fs in good agreement with the wavepacket dynamics reported by Tahara *et al.* [55]. In contrast ν_{21}, which is the mode associated with the pseudo Jahn-Teller (PJT) distortion, exhibits a strong transient signal that is out of phase with the features occurring in the ground state EXAFS spectrum (Figure S1), pointing to a damping of the EXAFS features in the excited state. It occurs because the excited state potential along this mode is flatter than the ground state, leading to a nuclear wavepacket that is more spread in the excited state. This additional width has the same dampening effect on the EXAFS spectrum as a Debye-Waller term [56].

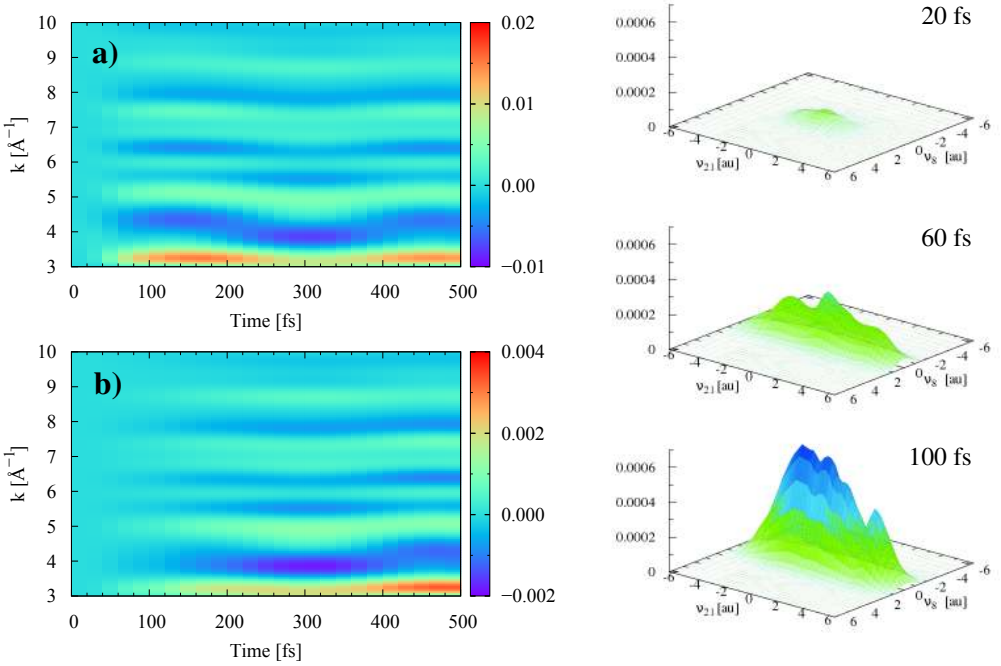

Figure 4. The simulated transient Cu K-edge EXAFS spectrum of $[Cu(dmp)_2]^+$ for the first 500 fs after photoexcitation calculated using the nuclear wavepacket dynamics occurring in the 2D nuclear coordinate space of ν_8 and ν_{21}. (a) The spectrum for the full nuclear wavepacket (b) The spectrum for the wavepacket dynamics in only the lowest triplet (T_1) state. The right hand side shows snapshots of the nuclear wavepacket in the T_1 state along the two modes at 20, 60 and 100 fs.

Figure 4a shows the simulated transient EXAFS spectrum using the nuclear wavepacket dynamics projected in the 2D nuclear coordinate space of ν_8 and ν_{21}. This shows a transient that has its main features out of phase with the ground state spectrum, but which is superimposed with the 300 fs oscillation associated with the wavepacket motion along ν_8. Due to the simplicity of the first coordination sphere, which is the dominant contribution to the EXAFS spectrum, this general structure is repeated at larger photoelectron energies (k), meaning that the experimental spectrum only needs to be recorded to $\sim$5 Å^{-1} ($\sim$9080 eV, $\sim$100 eV above the absorption edge). However, it is noted that in more complicated systems, with a less symmetric first coordination shell around the absorbing atom, different dynamics may well be reflect at different photoelectron energies, especially in the presence of heavier elements that scatter at larger k [57, 58].

As discussed in section 2.2, simulations of the EXAFS spectrum for the different excited states requires only the nuclear geometry. But this is not the case for the pre-edge region of the XAS spectrum and for the XES spectrum. For these cases, we investigate the ultrafast dynamics on the T_1 state only. Consequently to assess the effect of this approximation, Figure 4b shows the transient EXAFS spectrum using

nuclear wavepacket in the 2D nuclear coordinate space of ν_8 and ν_{21}, for which only the wavepacket on the T_1 has been considered. Importantly, the same wavepacket dynamics are observed, although the signal is a factor of ~5 weaker. This is due to the smaller (<30%) population (see Figure 1) of the T_1 state.

3.2. Pre-edge X-ray Absorption

Figure 5a shows the Cu K-edge pre-edge XANES spectrum in the ground and T_1 states (500 fs after photoexcitation) calculated using the 2D nuclear coordinate space of ν_8 and ν_{21}. The transient spectra simulated at every time-delay (τ) of 20 fs between τ=0 to 500 fs are shown in Figure S2. Ideally, one would wish to simulate the entire XANES spectrum. However, as a result of the difficulties associated with a quantitative description of these transient features [59], a quantitative agreement between the experimental spectrum recorded at a time-delay of 50 ps and the corresponding simulations [54] could not be achieved. Consequently, we focus upon the pre-edge region of the spectrum.

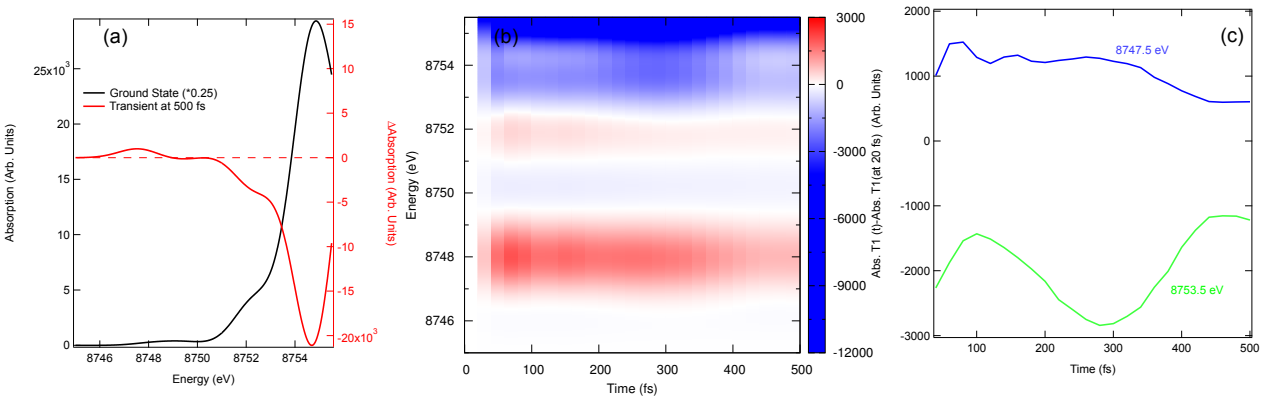

Figure 5. The simulated Cu K-edge pre-edge XANES spectrum for the dynamics in the lowest triplet T_1 state. (a) The ground state spectrum (scaled by 0.25) and transient spectrum of the wavepacket in the lowest triplet state 500 fs after photoexcitation (b) The transient changes changes in the lowest triplet state calculated using $T_1(\tau$ fs)-T_1(20 fs) (c) Time traces of (b) at 8745.5 eV and 8753.5 eV.

As reported in ref. [54], the transient spectrum (Figure 5a) shows the 2 main features, a weak positive feature 8747 eV that corresponds to a 1s→3d transition, and a strong negative feature that corresponds to a loss of intensity of the 1s-4p transition in the ground state spectrum. This latter feature is due to the blue shift of the absorption edge due to the oxidation state change of the metal centre upon population of the metal-to-ligand charge transfer state.

The spectral changes in the transient pre-edge XANES spectra are dominated

by the oxidation shift of the absorption edge and the change of the population of the T_1 (see Figure S2). As a consequence they do not exhibit any distinct changes associated with the wavepacket dynamics. To remove these two effects, Figure 5b shows the transient changes occurring in the T_1 state only, i.e. $T_1(\tau$ fs)-T_1(20 fs). Time traces at specific energies are shown in Figure 5c. The time-trace at 8753.5 eV, corresponding to just below the 1s-4p transition in the ground state spectrum, captures the oscillatory dynamics observed in the EXAFS spectra and exhibits a signal change $\sim$1%. Importantly, as the main features in the transient spectrum and the vibrational dynamics are unrelated, the energy region most sensitive to the wavepacket dynamics, in this case 8753.5 eV, does not necessarily correspond to the largest changes in the transient spectrum. Given the energy range considered here, we also cannot rule out these changes also occurring at higher energies in the XANES region of the spectrum, these will be significantly smaller than the transient changes associated with the 1s-4p transition and much closer to those of the EXAFS region.

3.3. X-ray emission

Figure 6a shows the K$\alpha_{1,2}$ XES spectra in the ground and 500 fs T_1 transient calculated using the 2D nuclear coordinate space. The transient spectra calculated every 20 fs between τ=0 to 500 fs are shown in Figure S3. The changes are small ($\sim$10%) and dominated by a shift in the emission energy associated with the change of spin state compared to the ground state [60]. This dominance of changing spin state is not surprising, as this core to core (2p$\rightarrow$1s) transition is not very sensitive to small changes in the molecular structure or valence electronic structure. Figures 6b and c again show the transient changes in the T_1 state and time traces at 7825 eV and 7844 eV. In this case, we do not observe any variations that can be associated with the nuclear wavepacket dynamics.

Figure 7 shows the corresponding plots for the K$\beta_{1,3}$ XES spectra. As this concerns transitions from 3p$\rightarrow$1s, it is likely to be more sensitive to the structural and valence electronic structural changes, especially via the 3p-3d exchange integral [61]. Indeed, while the transient spectra, shown in Figure 7a is again dominated by an edge shift (The transient spectra calculated every 20 fs between τ=0 to 500 fs are shown in Figure S4), Figures 7b and d reveal weak transient changes in the T_1 state and the 300 fs oscillatory period of the Cu-N totally symmetry stretch is observed. The magnitude of the changes associated with the wavepacket dynamics correspond to a $\sim$0.7% spectral change compared to the ground state spectrum, meaning that it has a similar magnitude change as the transient EXAFS signal.

Finally, Figure 8 shows the K$\beta_{2,5}$ XES spectra associated with the femtosecond dynamics in the T_1 state. In contrast to the K$\alpha_{1,2}$ and K$\beta_{1,3}$ XES the stronger effect of the wavepacket dynamics on the transient signal can be clearly observed in Figure 8b and c. This corresponds to a spectral change of $\sim$5% compared to the ground state spectrum and is about an order of magnitude larger than found for EXAFS, K$\alpha_{1,2}$ and K$\beta_{1,3}$

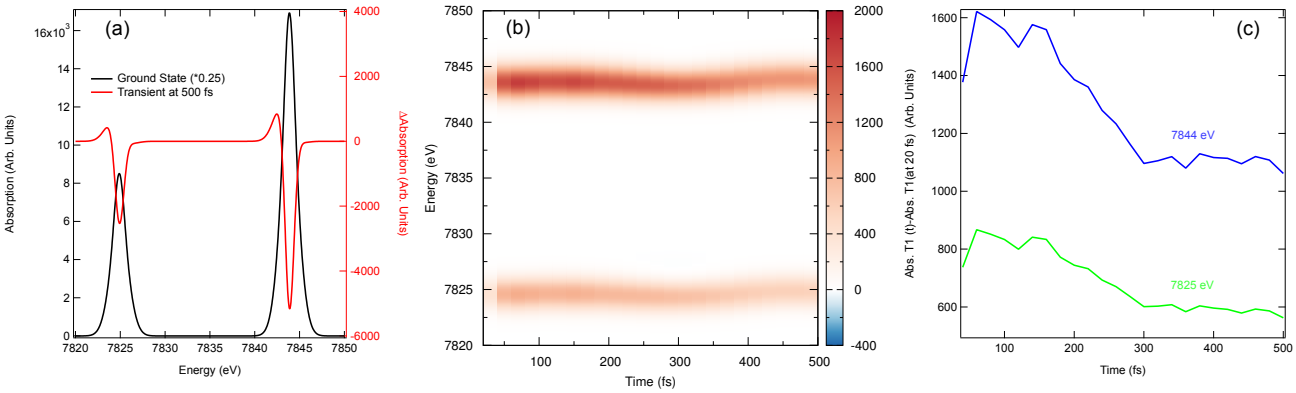

Figure 6. The simulated Cu K$\alpha_{1,2}$ XES spectrum for the dynamics in the lowest triplet T_1 state. (a) The ground state spectrum (scaled by 0.25) and transient spectrum of the wavepacket in the lowest triplet state 500 fs after photoexcitation (b) The transient changes changes in the lowest triplet state calculated using $T_1(\tau$ fs)-T_1(20 fs) (c) Time traces of (b) at 7825 eV and 7844 eV.

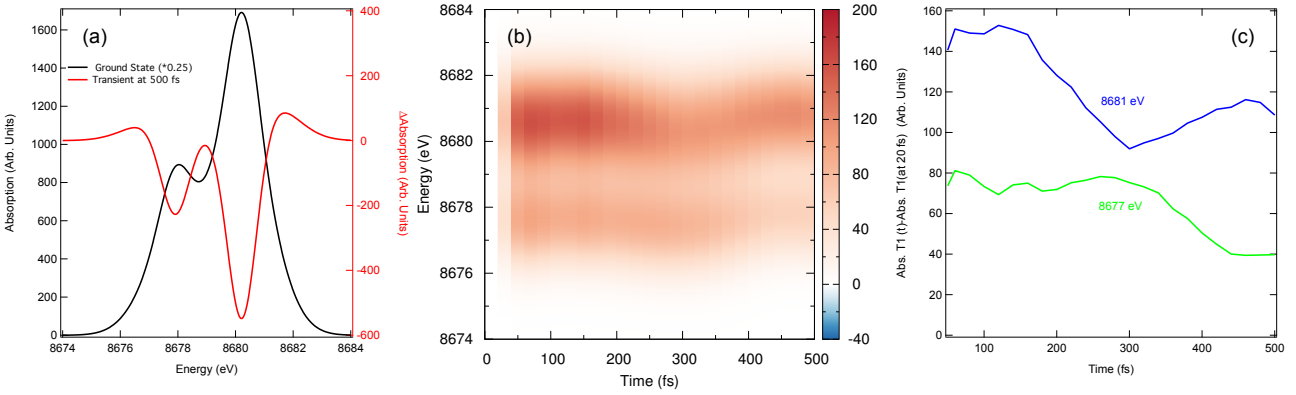

Figure 7. The simulated Cu K$\beta_{1,3}$ XES spectrum for the dynamics in the lowest triplet T_1 state. (a) The ground state spectrum (scaled by 0.25) and transient spectrum of the wavepacket in the lowest triplet state 500 fs after photoexcitation (b) The transient changes changes in the lowest triplet state calculated using $T_1(\tau$ fs)-T_1(20 fs) (c) Time traces of (b) at 8677 eV and 8681 eV.

XES. This highlights the distinct advantage and strong signals associated with directly probing the occupied valence density of states. However, the obvious disadvantage of this technique is, as discussed in the next section, the low cross sections, and therefore photon yields, associated with these transitions.

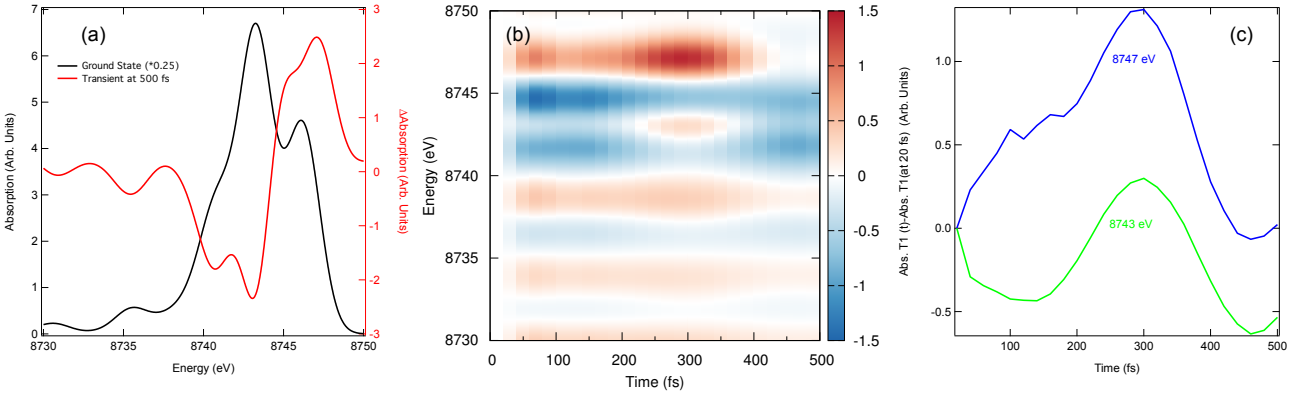

Figure 8. The simulated Cu K$\beta_{2,5}$ XES spectrum for the dynamics in the lowest triplet T_1 state. (a) The ground state spectrum (scaled by 0.25) and transient spectrum of the wavepacket in the lowest triplet state 500 fs after photoexcitation (b) The transient changes changes in the lowest triplet state calculated using $T_1(\tau$ fs)-T_1(20 fs) (c) Time traces of (b) at 8743 eV and 8747 eV.

3.4. Numerical Examples: Feasibility of Probing Wavepacket Dynamics

In the previous sections we have simulated the femtosecond EXAFS, pre-edge XANES and K$\alpha_{1,2}$, K$\beta_{1,3}$ and K$\beta_{2,5}$ XES spectra of photoexcited $[Cu(dmp)_2]^+$ using the nuclear wavepacket dynamics reported in refs [27, 28]. These have demonstrated that some of the signals (pre-edge XANES, EXAFS, K$\beta_{1,3}$ and K$\beta_{2,5}$) bear characteristics related to the wavepacket dynamics. However, the most crucial aspect of this work, regarding femtosecond laser-pump X-ray-probe experiments being used to investigate such dynamics is the X-ray photon flux required to achieve sufficient sensitivity to resolve these small spectral changes.

Many X-ray spectroscopic measurements are performed in fluorescence yield mode. For spectroscopies based upon the detection of scattered (fluorescent) photons, the spectra are formally represented within second order perturbation theory using the Kramers-Heisenberg equation:

$$F(\Omega,\omega) = \sum_f \sum_n \frac{\overbrace{\langle f|\hat{H}_{int}|n\rangle}^{\text{Emission}}\overbrace{\langle n|\hat{H}_{int}|i\rangle}^{\text{Absorption}}}{(E_i - E_n + \hbar\Omega)^2 + \frac{\Gamma_n^2}{4}} \times \frac{\Gamma_f/2\pi}{(E_i - E_f + \hbar\Omega - \hbar\omega)^2 + \Gamma_f^2/4}. \quad (1)$$

where $\hbar\Omega$ and $\hbar\omega$ are the incident and emitted photons, respectively and E_i, E_n, E_f are the energies of the initial, intermediate and final states. Γ_n and Γ_f are the lifetime broadening associated with the intermediate and final states. Here, we assume a non-coherent process, in which the absorption matrix elements from initial state i to intermediate state n, mediated by the interaction Hamiltonian $\hat{H}_i$, are weighted by the

emission matrix elements [11, 62].

For measurements of the XAS spectra, performed in total fluorescence yield (TFY) mode, the cross section of the absorption matrix element ($\langle n|\hat{H}_{int}|i\rangle$) at a particular X-ray incident energy is integrated over all of the emission matrix elements ($\langle f|\hat{H}_{int}|n\rangle$). Consequently, as discrimination of the energy of the emitted photons is not required, one can use a point detector, such as a silicon photodiode [20]. These can be placed close (∼15 mm) to the sample, and can therefore achieve a larger solid angle. Using the relation:

$$\theta = \frac{\pi r_{APD}^2}{4\pi R^2} \tag{2}$$

and assuming that the detector's active radius, r_{APD}=7mm the solid angle (θ) is ∼5%. Given the efficiency of the fluorescence process at Cu K-edge is ∼45% [63] and assuming a detector with a quantum efficiency of ∼0.8 [64, 65], we can combine these 3 components to yield a loss factor (of the photons in vs the photons out) of 2×10^{-2}.

In contrast, detection of the X-ray emission elements is proportional to the cross section of the absorption matrix element ($\langle n|\hat{H}_{int}|i\rangle$) multiplied by the cross section of the emission line of interest ($\langle f|\hat{H}_{int}|n\rangle$), i.e. $K\alpha_{1,2}$, $K\beta_{1,3}$. Consequently, the photon yield for each spectrum will be significantly lower making it harder to achieve a large signal to noise ratio (SNR) for these photon hungry techniques. In addition, for these experiments the X-ray emission spectrometer is further away from the sample causing additional losses and a smaller solid angle [60, 66]. For each emission line of interest, the fluorescence efficiency are Cu K$\alpha_{1,2}$=0.3, Cu K$\beta_{1,3}$-edge=0.03 and Cu K$\beta_{2,5}$-edge=0.00001 [63, 66]. Consequently given a reduced solid angle arising from the larger sample detector distance of $\theta \sim 0.04\%$ (∼5 millisteradians) [66, 67], the X-ray attenuation in air due to the larger distance from the detector [68], which is assumed to be 0.3, the total losses are Cu K$\alpha_{1,2}$-edge=3.0×10^{-5}, Cu K$\beta_{1,3}$-edge= 3.0×10^{-6} and Cu K$\beta_{2,5}$-edge = 9.6×10^{-9}.

Assuming a 100 μm thick jet of 25 mM solution, the absorbed fraction of photons, according to the Beer-Lambert law is ∼2%. It is stressed that this approximation is only strictly valid for solvents containing light elements (e.g., water, acetonitrile, hexane) and may change for heavier solvents, like CCl_4 [65]. With these conditions in mind, given 10^{10} photons per pulse achievable for the monochromatic mode of the LCLS [69], the number of useful photons per pulse detected (see Table 1), i.e. once the loss factors have been included, is: 4×10^6 (TFY), 6×10^3 (Cu K$\alpha_{1,2}$), 6.0×10^2 (Cu K$\beta_{1,3}$) and 2.0×10^0 (Cu K$\beta_{2,5}$).

In an experiment, provided that most of the electronic noise is suppressed, the detection sensitivity can be close to the shot-noise limit. This inherent noise is given as $\sqrt{N}$, where N is the signal, i.e. the number of photons detected. The signal to noise ratio is therefore given SNR=N/$\sqrt{N}$. Using these boundary conditions, Table 1 shows the number of X-ray photons, and consequently of X-ray pulses, required to measure with a SNR=10 for i) a transient X-ray spectroscopic signal and ii) the wavepacket dynamics. The number of X-ray photons (I^{Npho}) required to measure a given signal

	Photons Out Per Pulse	$\Delta\chi$ (Signal)	I^{Npho} (N_{shots})	$\Delta\chi$ (WP)	I^{Npho} (N_{shots})
TFY XANES	4.0×10^6	$0.60^\dagger$	3.0×10^4 (1)	$0.01^\dagger$	1×10^8 (25)
TFY EXAFS	4.0×10^6	0.01	1.0×10^8 (25)	0.003	1×10^9 (250)
K$\alpha_{1,2}$	6.0×10^3	0.10	1.0×10^6 (170)	-	-
K$\beta_{1,3}$	6.0×10^2	0.20	2.5×10^5 (425)	0.007	2.0×10^8 (3.5×10^5)
K$\beta_{2,5}$	2.0×10^0	0.40	6.3×10^4 (3.2×10^4)	0.050	4×10^6 (2.0×10^6)

Table 1. The number of X-ray photons (I^{Npho}) and the number (N_{shots}) of X-ray pulses (10^{10} photons per pulse) required to observe the transient $\Delta\chi$ associated with a normal pump-probe signal (signal) and to directly observe the wavepacket dynamics (WP). The photolysis yield f is assumed to be 10% throughout. †: This is only valid for the 1s-4p transition in the XANES region. Other changes are smaller and the pre-edge, being dipole forbidden 1s-3d transitions is significantly smaller and much closer to the spectral changes observed in the EXAFS region of the spectrum.

scales as [65]:

$$I^{Npho} \propto \left[\frac{SNR}{f\cdot\Delta\chi}\right]^2 \tag{3}$$

where $\Delta\chi$ is the signal change and f is the photolysis yield assumed to be 10% throughout. Using $I^0=10^{10}$ as the incoming X-ray intensity (number of photons per pulse), the loss factor (L) and the fraction of absorbed photons (μ_A), we can use Equation 3 to estimate the number of X-ray pulses (N_{shots}) required with:

$$N_{shots} = \frac{I^{Npho}}{I_0\cdot\mu_A\cdot L} \tag{4}$$

Using Equations 3 and 4, Table 1 shows that to record a transient signal pump-probe using TFY XANES or TFY EXAFS requires $\sim 3.0\times10^4$ and $\sim1.0\times10^8$ photons, respectively. Given that the number of detected photons/pulse detected is 4×10^6, this makes it plausible for each data point of TFY XANES to be recorded with a SNR=10 within a single X-FEL pulse. TFY EXAFS requires ~25 X-ray pulses, however this still means that each data point can be collected with <1 s of acquisition time (assuming a 100 Hz repetition rate). In contrast, due to smaller $\Delta\chi$ associated with resolving the spectral fluctuations of wavepacket dynamics a larger number of photons is required. Indeed, to achieve a SNR=10, for TFY XANES and TFY EXAFS each data point would be expected to require ~25 and ~250 X-ray pulses, respectively. Importantly, this is still achievable within a reasonable data acquisition time (<4 s per data point).

Table 1 also shows the number of photons required to achieve a transient signal, $\Delta\chi$ for K$\alpha_{1,2}$, K$\beta_{1,3}$ and K$\beta_{2,5}$ XES. While these photon hungry techniques are difficult to implement in a time-resolved manner at 3^{rd} generation synchrotrons [60, 67], the increased photon flux associated with the X-FELs makes these feasible in the sub-ps regime. Indeed, for the hardest case, K$\beta_{2,5}$ XES, it is expected that $\sim3.2\times10^4$ X-ray pulses per data point is required. Given the repetition rate of X-FELs (~100 Hz), this

would require acquisition times of ∼10-20 mins per data point. For these experiments the potentially high X-ray fluency and repetition rate of the European X-FEL could make such measurements significantly easier [70]. However, Table 1 shows that although measuring the transient signal is possible even for K$\beta_{2,5}$ XES, the number of X-ray pulses, $\sim 10^{5-6}$ required to achieve sufficient SNR to observe the wavepacket dynamics with these spectroscopies makes them completely unfeasible (∼6 hours per data point at 100 Hz).

4. Discussions and Conclusions

Ultrafast time-resolved linear and non-linear optical spectroscopies have a strong history of providing important insight into photoexcited dynamics within the femtosecond regime. Owing to the development of the X-FELs, these dynamics can now also be observed in the short-wavelength regime and provide direct snapshots of interatomic distances and changes in charge distribution of molecules. These techniques hold great promise of yielding important new insight into fundamental dynamical processes such as vibrational excitation, bond formation and breaking, relaxation, and time-dependent solvation processes.

In this paper we have used wavepacket dynamics simulations to predict femtosecond EXAFS, pre-edge XANES, K$\alpha_{1,2}$, K$\alpha_{1,3}$ and K$\beta_{2,5}$ XES spectra. These have demonstrated that for the present system, femtosecond pre-edge XANES, EXAFS, K$\beta_{1,3}$ and K$\beta_{2,5}$ XES spectra all reveal information about the wavepacket dynamics. However using realistic experimental parameters, while it will be possible to record a signal capturing the strongest transient changes for all of the spectroscopies studies herein, we have demonstrated that the wavepacket dynamics can only be observed experimentally within realistic acquisition times for XANES and EXAFS, as the small cross section associated with K$\beta_{1,3}$ and K$\beta_{2,5}$ XES makes the number of X-ray pulses required unfeasible.

In the present study we have not considered L-edge spectroscopy. However recent work has demonstrated that it is possible to record high quality L-edge spectra of dilute 3d transition metals using a high transmission zone-plate spectrometer implemented at the Linac Coherent Light Source (LCLS). [71] Although the L-edges have a smaller fluorescence yield (∼10%), these transitions (2p-3d) could be a interesting alternative approach that should also be explored.

Importantly, in terms of a general feasibility, the transient signals for the present case $[Cu(dmp)_2]^+$ are dominated by an oxidation shift associated with the charge transfer of an electron from the metal to the ligands upon excitation. As this has no correspondence with the wavepacket dynamics, the changes associated with these vibrational coherences will be a small change on top of the large underlying transient of the edge shift. This means that resolving the wavepacket dynamics for the present system represents a challenging case. Given that it remains possible, this holds significant promise for future experiments in this area. It should be stressed that as the

main features in the transient spectrum and the vibrational dynamics are unrelated, the energy region most sensitive to the wavepacket dynamics does not necessarily correspond to the largest changes in the transient spectrum making it important to record the whole spectrum at each time-delay and not just a time scan at one particular energy. For other cases, such as $[Fe(bpy)_3]^{2+}$ [15, 72, 73, 60, 74] determining the wavepacket dynamics could be expected to be easier. In this case, the transient spectrum is not dominated by a feature unrelated to the vibrational coherences. Instead, here the wavepacket dynamics reported by Chergui and co-workers [75] occurs along this Fe-N coordinate, which is also responsible for the principal transient changes in the Fe K-edge XAS spectrum. In this case the wavepacket dynamics would therefore be expected to yield larger changes making observing these dynamics easier. This highlights the strong emphasis that should be placed upon fully understanding the dominant contributions to a transient signal at longer times (i.e. using a 3^{rd} generation synchrotrons) before determining if a particular experiment is possible.

Acknowledgments

We thank the Swiss National Science Foundation (Grant 200021-137717) and the NCCR MUST for funding.

5. References

[1] A H Zewail. Laser Femtochemistry. *Science*, 242(4886):1645–1653, 1988.

[2] Shaul Mukamel. *Principles of nonlinear optical spectroscopy*. Oxford University Press, USA, 1995.

[3] David A Reis and Aaron M Lindenberg. Ultrafast X-ray scattering in solids. *Light Scattering In Solids IX*, 108:371–422, 2007.

[4] Thomas Elsaesser and Michael Woerner. Photoinduced structural dynamics of polar solids studied by femtosecond X-ray diffraction. *Acta Crystallographica Section A*, 66:168–178, 2010.

[5] S. L. Johnson, P Beaud, E Vorobeva, C J Milne, E D Murray, S Fahy, and G Ingold. Non-equilibrium phonon dynamics studied by grazing-incidence femtosecond X-ray crystallography. *Acta Crystallographica Section A*, 66:157–167, 2010.

[6] Germán Sciaini and R J Dwayne Miller. Femtosecond electron diffraction: heralding the era of atomically resolved dynamics. *Reports on Progress in Physics*, 74:096101, 2011.

[7] Majed Chergui and Ahmed H Zewail. Electron and X-Ray Methods of Ultrafast Structural Dynamics: Advances and Applications. *ChemPhysChem*, 10(1):28–43, 2009.

[8] TJ Penfold, CJ Milne, and M Chergui. Recent advances in ultrafast x-ray absorption spectroscopy of solutions. *Advances. in Chemical Physics*, 153:1–41, 2013.

[9] Christian Bressler and Majed Chergui. Molecular Structural Dynamics Probed by Ultrafast X-Ray Absorption Spectroscopy. *Annual Review Of Physical Chemistry*, 61:263–282, 2010.

[10] LX Chen. Probing transient molecular structures with time-resolved pump/probe XAFS using synchrotron X-ray sources. *Journal of Electron Spectroscopy and Related Phenomena*, 119(2):161–174, 2001.

[11] C.J. Milne, T.J. Penfold, and M. Chergui. Recent experimental and theoretical developments intime-resolved x-ray spectroscopies. *Coordination Chemistry Reviews*, (0):–, 2014.

[12] AH Zewail. 4D ultrafast electron diffraction, crystallography, and microscopy. *Annual Review Of Physical Chemistry*, 57:65–103, 2006.

[13] Renske M van der Veen, Thomas J Penfold, and Ahmed H Zewail. Ultrafast core-loss spectroscopy in four-dimensional electron microscopy. *Structural Dynamics*, 2(2):024302, 2015.

[14] RW Schoenlein, S Chattopadhyay, HHW Chong, TE Glover, PA Heimann, CV Shank, AA Zholents, and MS Zolotorev. Generation of femtosecond pulses of synchrotron radiation. *Science*, 287(5461):2237–2240, 2000.

[15] Christian Bressler, Christopher J Milne, Van-Thai Pham, Amal el Nahhas, Renske M van der Veen, Wojciech Gawelda, Steven Lee Johnson, Paul Beaud, Daniel Grolimund, Maik Kaiser, Camelia N Borca, Gerhard Ingold, Rafael Abela, and Majed Chergui. Femtosecond XANES Study of the Light-Induced Spin Crossover Dynamics in an Iron(II) Complex. *Science*, 323(5913):489–492, 2009.

[16] N Huse, H Cho, K Hong, L Jamula, FMF de Groot, TK Kim, JK McCusker, and RW Schoenlein. Femtosecond Soft X-ray Spectroscopy of Solvated Transition-Metal Complexes: Deciphering the Interplay of Electronic and Structural Dynamics. *The Journal of Physical Chemistry Letters*, 2:880–884, 2011.

[17] Van-Thai Pham, Thomas J Penfold, Renske M van der Veen, Frederico Lima, Amal el Nahhas, Steve L Johnson, Paul Beaud, Rafael Abela, Christian Bressler, Ivano Tavernelli, Christopher J Milne, and Majed Chergui. Probing the Transition from Hydrophilic to Hydrophobic Solvation with Atomic Scale Resolution. *Journal Of The American Chemical Society*, 133(32):12740–12748, 2011.

[18] A Cavalleri, M Rini, HHW Chong, S Fourmaux, TE Glover, PA Heimann, JC Kieffer, and RW Schoenlein. Band-selective measurements of electron dynamics in vo 2 using femtosecond near-edge x-ray absorption. *Physical review letters*, 95(6):067405, 2005.

[19] S Khan. Free-electron lasers. *Journal of Modern Optics*, 55(21):3469–3512, 2008.

[20] Henrik T Lemke, Christian Bressler, Lin X Chen, David M Fritz, Kelly J Gaffney, Andreas Galler, Wojciech Gawelda, Kristoffer Haldrup, Robert W Hartsock, Hyotcherl Ihee, Jeongho Kim, Kyung Hwan Kim, Jae Hyuk Lee, Martin M Nielsen, Andrew B Stickrath, Wenkai Zhang, Diling Zhu, and Marco Cammarata. Femtosecond X-ray Absorption Spectroscopy at a Hard X-ray Free Electron Laser: Application to Spin Crossover Dynamics. *The Journal of Physical Chemistry A*, 117(4):735–740, 2013.

[21] Wenkai Zhang, Roberto Alonso-Mori, U. Bergmann, C Bressler, M Chollet, Andreas Galler, W Gawelda, Ryan G Hadt, Robert W. Hartsock, Thomas Kroll, Kasper S Kjaer, Katharina Kubiček, Henrik T Lemke, Huiyang W Liang, Drew A Meyer, Martin M Nielsen, Carola Purser, Joseph S Robinson, EI Solomon, Zheng Sun, Dimosthenis Sokaras, Tim B van Driel, G Vanko, Tsu-Chien Weng, Diling Zhu, and K J Gaffney. Tracking excited-state charge and spin dynamics in iron coordination complexes. *Nature*, 509(7500):345–348, May 2014.

[22] Marco Cammarata, Roman Bertoni, Maciej Lorenc, Hervé Cailleau, Sergio Di Matteo, Cindy Mauriac, Samir F Matar, Henrik Lemke, Matthieu Chollet, Sylvain Ravy, et al. Sequential activation of molecular breathing and bending during spin-crossover photoswitching revealed by femtosecond optical and x-ray absorption spectroscopy. *Physical review letters*, 113(22):227402, 2014.

[23] Y Ogi, Y Obara, T Katayama, Y-I Suzuki, SY Liu, NC-M Bartlett, N Kurahashi, S Karashima, T Togashi, Y Inubushi, et al. Ultraviolet photochemical reaction of [fe (iii)(c2o4) 3] 3- in aqueous solutions studied by femtosecond time-resolved x-ray absorption spectroscopy using an x-ray free electron laser. *Structural Dynamics*, 2(3):034901, 2015.

[24] Ph Wernet, K Kunnus, I Josefsson, I Rajkovic, W Quevedo, M Beye, S Schreck, S Grubel, M Scholz, D Nordlund, W Zhang, R W Hartsock, W F Schlotter, J J Turner, B Kennedy, F Hennies, F M F de Groot, K J Gaffney, S Techert, M Odelius, and A Föhlisch. Orbital-specific mapping of the ligand exchange dynamics of Fe(CO)5 in solution. *Nature*, 520(7545):78–81, April 2015.

[25] Albert Stolow, Arthur E Bragg, and Daniel M Neumark. Femtosecond time-resolved photoelectron spectroscopy. *Chemical reviews*, 104(4):1719–1758, 2004.

[26] Shaul Mukamel. Femtosecond optical spectroscopy: a direct look at elementary chemical events.

Annual Review of Physical Chemistry, 41(1):647–681, 1990.

[27] G Capano, T J Penfold, U Rothlisberger, and I Tavernelli. A Vibronic Coupling Hamiltonian to describe the ultrafast excited state dynamics of a Cu(I)-phenanthroline complex. *Chimia*, 68:227–230, 2014.

[28] Gloria Capano, Majed Chergui, Ursula Rothlisberger, Ivano Tavernelli, and Thomas James Penfold. A quantum dynamics study of the ultrafast relaxation in a prototypical cu(i)-phenanthroline. *The Journal of Physical Chemistry A*, 0(ja):null, 2014.

[29] LX Chen, GB Shaw, I Novozhilova, T Liu, G Jennings, K Attenkofer, GJ Meyer, and P Coppens. MLCT state structure and dynamics of a copper(I) diimine complex characterized by pump-probe X-ray and laser spectroscopies and DFT calculations. *Journal Of The American Chemical Society*, 125:7022–7034, 2003.

[30] ZA Siddique, Y Yamamoto, T Ohno, and K Nozaki. Structure-dependent photophysical properties of singlet and triplet metal-to-ligand charge transfer states in copper(I) bis(diimine) compounds. *Inorganic Chemistry*, 42(20):6366–6378, 2003.

[31] George B Shaw, Christian D Grant, Hideaki Shirota, Edward W CASTNER, Gerald J Meyer, and Lin X Chen. Ultrafast structural rearrangements in the MLCT excited state for copper(I) bis-phenanthrolines in solution. *Journal Of The American Chemical Society*, 129(7):2147–2160, 2007.

[32] M Iwamura, S Takeuchi, and T Tahara. Real-time observation of the photoinduced structural change of bis(2,9-dimethyl-1,10-phenanthroline)copper(I) by femtosecond fluorescence spectroscopy: A realistic potential curve of the Jahn-Teller distortion. *Journal Of The American Chemical Society*, 129:5248–5256, 2007.

[33] M Iwamura, H Watanabe, K Ishii, S Takeuchi, and T Tahara. Coherent Nuclear Dynamics in Ultrafast Photoinduced Structural Change of Bis (diimine) copper (I) Complex. *J. Am. Chem. Soc.*, 133:7728, 2011.

[34] M Iwamura, S Takeuchi, and Tahara, T. Substituent effect on the photoinduced structural change of Cu(I) complexes observed by femtosecond emission spectroscopy. *Physical Chemistry Chemical Physics*, 16(9):4143–4154, 2014.

[35] H.-D. Meyer, U. Manthe, and L. S. Cederbaum. The multi-configurational time-dependent Hartree approach. *Chemical Physics Letter*, 165:73–78, 1990.

[36] M. H. Beck, A. Jäckle, G. A. Worth, and H.-D. Meyer. The multiconfiguration time-dependent Hartree method: A highly efficient algorithm for propagating wavepackets. *Phys. Rep.*, 324:1–105, 2000.

[37] H. Köppel, W. Domcke, and L. S. Cederbaum. Multimode molecular dynamics beyond the Born-Oppenheimer approximation. 57:59–246, 1984.

[38] Ida Josefsson, Kristjan Kunnus, Simon Schreck, Alexander Föhlisch, Frank de Groot, Philippe Wernet, and Michael Odelius. Ab Initio Calculations of X-ray Spectra: Atomic Multiplet and Molecular Orbital Effects in a Multiconfigurational SCF Approach to the L-Edge Spectra of Transition Metal Complexes. *The Journal of Physical Chemistry Letters*, pages 3565–3570, 2012.

[39] Nicholas A Besley, Andrew T B Gilbert, and Peter M W Gill. Self-consistent-field calculations of core excited states. *The Journal of Chemical Physics*, 130(12):124308, 2009.

[40] Nicholas A Besley, Equation of motion coupled cluster theory calculations of the X-ray emission spectroscopy of water. *Chem. Phys. Lett.*, 542:42-46, 2012.

[41] JJ Rehr, JJ Kas, MP Prange, AP Sorini, Y Takimoto, and F Vila. Ab initio theory and calculations of X-ray spectra. *Comptes Rendus Physique*, 10:548, 2009.

[42] Martha A Beckwith, Michael Roemelt, Marie-Noëlle Collomb, Carole DuBoc, Tsu-Chien Weng, Uwe Bergmann, Pieter Glatzel, Frank Neese, and Serena DeBeer. Manganese kβ x-ray emission spectroscopy as a probe of metal–ligand interactions. *Inorganic chemistry*, 50(17):8397–8409, 2011.

[43] Nicole Lee, Taras Petrenko, Uwe Bergmann, Frank Neese, and Serena DeBeer. Probing valence

orbital composition with iron kβ x-ray emission spectroscopy. *Journal of the American Chemical Society*, 132(28):9715–9727, 2010.

[44] Frank Neese. The ORCA program system. *Wiley Interdisciplinary Reviews-Computational Molecular Science*, 2(1):73–78, 2012.

[45] AD Becke. Density-functional exchange-energy approximation with correct asymptotic behavior. *Phys. Rev. A*, 38:3098–3100, 1988.

[46] J. P Perdew. Density-Functional Approximation for the Correlation-Energy of the Inhomogeneous Electron-Gas. *Physical Review B*, 33:8822–8824, 1986.

[47] Ansgar Schäfer, Hans Horn, and Reinhart Ahlrichs. Fully optimized contracted gaussian basis sets for atoms li to kr. *The Journal of Chemical Physics*, 97(4):2571–2577, 1992.

[48] Florian Weigend and Reinhart Ahlrichs. Balanced basis sets of split valence, triple zeta valence and quadruple zeta valence quality for h to rn: design and assessment of accuracy. *Physical Chemistry Chemical Physics*, 7(18):3297–3305, 2005.

[49] Bernd A Hess, Christel M Marian, Ulf Wahlgren, and Odd Gropen. A mean-field spin-orbit method applicable to correlated wavefunctions. *Chemical Physics Letters*, 251(5):365–371, 1996.

[50] M Stener. Time dependent density functional theory of core electrons excitations. *Chemical Physics Letters*, 373(1-2):115–123, 2003.

[51] NA Besley, MJG Peach, and DJ Tozer. Time-dependent density functional theory calculations of near-edge X-ray absorption fine structure with short-range corrected functionals. *Physical Chemistry Chemical Physics*, 11(44):10350, 2009.

[52] S DeBeer-George, T Petrenko, and F Neese. Prediction of Iron K-Edge Absorption Spectra Using Time-Dependent Density Functional Theory. *Journal Of Physical Chemistry A*, 112:12936–12943, 2008.

[53] G Capano, T J Penfold, N A Besley, C J Milne, M Reinhard, H Rittmann-Frank, P Glatzel, Rafael Abela, U Rothlisberger, M Chergui, and I Tavernelli. The role of Hartree-Fock exchange in the simulation of X-ray absorption spectra: A study of photoexcited $[Fe(bpy)_3]^{2+}$. *Chemical Physics Letters*, 580:179–184, 2013.

[54] T J Penfold, S Karlsson, G Capano, F A Lima, J Rittmann, M Reinhard, M H Rittmann-Frank, O Braem, E Baranoff, Rafael Abela, I Tavernelli, U Rothlisberger, C J Milne, and M Chergui. Solvent-Induced Luminescence Quenching: Static and Time-Resolved X-Ray Absorption Spectroscopy of a Copper(I) Phenanthroline Complex. *The Journal of Physical Chemistry A*, 117(22):4591–4601, 2013.

[55] Munetaka Iwamura, Satoshi Takeuchi, and Tahei Tahara. Ultrafast excited-state dynamics of copper (i) complexes. *Accounts of chemical research*, 48(3):782–791, 2015.

[56] Bret Jackson and Horia Metiu. An examination of the use of wave packets for the calculation of atom diffraction by surfaces. *The Journal of chemical physics*, 82(12):5707–5716, 1985.

[57] DC Koningsberger, BL Mojet, GE Van Dorssen, and DE Ramaker. XAFS spectroscopy; fundamental principles and data analysis. *Topics in catalysis*, 10(3):143–155, 2000.

[58] T J Penfold, I Tavernelli, C J Milne, M Reinhard, A El Nahhas, Rafael Abela, U Rothlisberger, and M Chergui. A wavelet analysis for the X-ray absorption spectra of molecules. *The Journal of Chemical Physics*, 138(1):014104, 2013.

[59] JJ Rehr and RC Albers. Theoretical approaches to x-ray absorption fine structure. *Reviews Of Modern Physics*, 72(3):621–654, 2000.

[60] Gyorgy Vankó, A Bordage, P Glatzel, E Gallo, M Rovezzi, W Gawelda, A Galler, C Bressler, G Doumy, A M March, E P Kanter, L Young, S H Southworth, S E Canton, J Uhlig, G Smolentsev, V Sundstrom, K. Haldrup, T B van Driel, M. M. Nielsen, K S Kjær, and H. T. Lemke. Spin-state studies with XES and RIXS: From static to ultrafast. *Journal Of Electron Spectroscopy And Related Phenomena*, 188:166–171, 2013.

[61] Frank de Groot. High-Resolution X-ray Emission and X-ray Absorption Spectroscopy. *Chemical Reviews*, 101(6):1779–1808, 2001.

[62] F De Groot and A Kotani. *Core Level Spectroscopy of Solids*. *CRC Press*, 2008.

[63] MO Krause. Natural widths of atomic K and L levels, Ka X-ray lines and several KLL Auger lines. *J Phys Chem Ref Data*, 1979.

[64] W Gawelda. Time-resolved x-ray absorption spectroscopy of transition metal complexes. *EPFL Thesis*, pages 1–307, November 2006.

[65] Christian Bressler and Majed Chergui. Ultrafast X-ray absorption spectroscopy. *Chemical Reviews*, 104:1781–1812, 2004.

[66] J. Szlachetko, M Nachtegaal, E de Boni, M Willimann, O Safonova, J Sa, G Smolentsev, M. Szlachetko, J. A. van Bokhoven, J. Cl. Dousse, J Hoszowska, Y Kayser, P Jagodzinski, A Bergamaschi, B Schmitt, C David, and A Lücke. A von Hamos x-ray spectrometer based on a segmented-type diffraction crystal for single-shot x-ray emission spectroscopy and time-resolved resonant inelastic x-ray scattering studies. *Review Of Scientific Instruments*, 83(10):103105, 2012.

[67] Anne Marie March, Tadesse A Assefa, Christian Bressler, Gilles Doumy, Andreas Galler, Wojciech Gawelda, Elliot P Kanter, Zoltán Németh, Mátyás Pápai, Stephen H Southworth, et al. Feasibility of valence-to-core x-ray emission spectroscopy for tracking transient species. *The Journal of Physical Chemistry C*, 2015.

[68] Uwe Bergmann and Pieter Glatzel. X-ray emission spectroscopy. *Photosynthesis research*, 102(2-3):255–266, 2009.

[69] John D Bozek. Amo instrumentation for the lcls x-ray fel. *The European Physical Journal-Special Topics*, 169(1):129–132, 2009.

[70] Massimo Altarelli, R Brinkmann, M Chergui, W Decking, B Dobson, S Düsterer, G Grübel, W Graeff, H Graafsma, J Hajdu, et al. The european x-ray free-electron laser. *Technical Design Report, DESY*, 97:2006, 2006.

[71] R. Mitzner, J. Rehanek, J Kern, S Gul, J. Hattne, T. Taguchi, R Alonso-Mori, R Tran, C Weniger, H. Schrder *et al.* L-edge X-ray absorption spectroscopy of dilute systems relevant to metalloproteins using an X-ray free-electron laser. In *Journal of Physical Chemistry Letters*, 4:3641–3647, 2013

[72] A Cannizzo, C J Milne, C Consani, W Gawelda, Ch Bressler, F van Mourik, and M Chergui. Light-induced spin crossover in Fe(II)-based complexes: The full photocycle unraveled by ultrafast optical and X-ray spectroscopies. In *Coordination Chemistry Reviews*, 254:2677–2686, 2010.

[73] W Gawelda, V T Pham, R M van der Veen, D Grolimund, Rafael Abela, M Chergui, and C Bressler. Structural analysis of ultrafast extended x-ray absorption fine structure with subpicometer spatial resolution: Application to spin crossover complexes. *The Journal of Chemical Physics*, 130(12):124520, 2009.

[74] K. Haldrup, G Vankó, W Gawelda, A Galler, G Doumy, A M March, E P Kanter, A Bordage, A Dohn, T B van Driel, K S Kjær, H. T. Lemke, S E Canton, J Uhlig, V Sundstrom, L Young, S H Southworth, M. M. Nielsen, and C Bressler. Guest–Host Interactions Investigated by Time-Resolved X-ray Spectroscopies and Scattering at MHz Rates: Solvation Dynamics and Photoinduced Spin Transition in Aqueous Fe(bipy)$_3^{2+}$. *The Journal of Physical Chemistry A*, 116(40):9878–9887, 2012.

[75] Cristina Consani, Mirabelle Prémont-Schwarz, Amal ElNahhas, Christian Bressler, Frank van Mourik, Andrea Cannizzo, and Majed Chergui. Vibrational Coherences and Relaxation in the High-Spin State of Aqueous [Fe^{II}(bpy)$_3$]$^{2+}$. *Angewandte Chemie International Edition*, 48(39):7184–7187, 2009.